

# 矽-基底之電晶體於高頻特性的可靠度分析

研究生：黃聖懿


指導教授：張俊彥 院士

陳坤明 博士

國立交通大學

電子工程學系 電子研究所博士班

## 中文摘要



近年來，隨著無線通訊技術的快速發展以及電路成本上的降低，矽-基底之電晶體在實行系統整合於單一晶片的角色及運用也越來越趨成熟。在開發先進元件的同時，可靠度的測試和分析也將會是一個重要的議題。而傳統上直流所做的參數的可靠度測試，是否就能符合高頻電路操作下的相對安全規格？亦或是高頻電路操作下，主動元件所需考量的可靠度因素會比傳統上所做的直流測試更加嚴苛？這些考量的因素在於直流測試以及高頻測試之間的關聯性又是如何？

本論文的研究方向和主題即是針對於這個有趣的議題在矽基底電晶體的高頻操作運用上，做一個有系統並且完整的分析。論文中，針對矽基底電晶體的部分則是包含兩大主題：矽鍺異質接面雙極性電晶體

(SiGe HBTs)、以及金氧半場效電晶體 (MOSFETs)。

傳統上，針對矽鍺異質接面雙極性電晶體的可靠度測試主要的方法可再細分為兩種：反向偏壓的射極-基極接面 (Reverse-biased Emitter-Base junctions, and left collector open)，與順向偏壓集極電流 (Forward-biased Collector current)，而相同的目的即是利用相對較高的電壓或是電流的驅迫 (Stressing)，來產生較大的電場以及帶有較高能量的熱載子。近年來，由於矽鍺異質接面雙極性電晶體主要運用於高頻電路中的功率電路 (Power Amplifier)，而在接近實際操作情況下，同時產生較高的輸出電流以及較高的輸出電壓，而這樣的偏壓條件下，也對於元件的可靠度是一個新的挑戰。而所謂的混合驅迫 (Mixed-Mode Stressing) 就是利用矽鍺異質接面雙極性電晶體在操作的同時給於較高的電流密度以及高電壓下所造成的一種熱載子驅迫。這個接近實際操作下的熱載子分析，也是本論中高頻可靠度分析的一項重要主軸，尤其是在高頻功率上所造成的影響。

傳統的反向偏壓射極-基極接面驅迫所造成的熱載子會在靠近基極和射極接面以及隔離基極-射極的絕緣層上產生接面陷阱 (traps) 和帶電荷的接面態 (interface state)，而影響其直流特性上的電性反應。譬如在基極電流上產生非理想的複合漏電流，而造成電流增益的下降。這也會影響高頻操作時某些可預期的電性上的劣化反應。在此實驗中，

由於熱載子對於基極電流和集極電流所造成的影響並不一致，所以我們也針對於不同方式的電流驅動下(固定  $I_C$  和 固定  $I_B$ )，完整地分析熱載子對於矽鍺異質接面雙極性電晶體實際操作上，在其高頻特性以及功率特性的影響。並以小訊號等效電路將其參數萃出作為分析比較以及尋找出高頻參數的劣化與直流特性參數劣化之間的相關性。而在混合驅迫下，熱載子對於矽鍺異質接面雙極性電晶體所造成的傷害，除了直流上的變異，高頻操作下我們則是利用大訊號(VBIC)模型，將其相關的參數萃出，並對於高頻特性、功率特性做一個完整的分析和功率放大器的模擬。並且在這實驗的過程中，我們發現在固定集極電流驅動下的矽鍺異質接面雙極性電晶體，受到熱載子傷害後，其高頻特性以及功率特性相對地較不受到影響。



另一方面，本論文也針對金氧半場效電晶體的高頻操作下的可靠度做了一個完整的分析。而本論文中，對於金氧半場效電晶體的可靠度的討論則是包含了熱載子傷害以及閘極氧化層的崩潰。其中，我們分析探討的範圍包含了高頻電路運用下的幾個主要規格，例如：截止頻率、最大震盪頻率、雜訊指數、線性度以及高頻功率。並且在實驗的過程中，我們發現一般直流劣化的參數並不足以提供和代表高頻操作下規格劣化的指標。所以在我們這完整的分析裡，我們建議高頻可靠度的模型必須重新被建立。

# **Reliability and Characterizations on the Silicon-Based Transistors for High-Frequency Applications**

Student: Sheng-Yi Huang

Advisors: Prof. Chun-Yen Chang  
Dr. Kun-Ming Chen

A Dissertation

Department of Electronics Engineering and Institute of Electronics National  
Chiao Tung University, Hsinchu, Taiwan

## **Abstract**

In recent years, with the advanced technologies in communication system, silicon-based transistors have played an important role; especially, for low-cost and highly-integration system-on-a-chip (SOC). In the development of such advanced devices, the analysis of reliability becomes the most important concern. It is a question, if the DC parameters of reliability can guarantee the reliable operation in RF circuits? Or the reliability issues should be considered more carefully in the RF parameters than those in DC parameters. As to the device reliabilities, we are curious about the interaction and the co-relation between the DC degraded parameters and the RF parameters.

We examined and analyzed the interesting reliability issues on the silicon-based transistors; especially, for the high-frequency operation in this thesis. As to the topic of silicon-based transistors, we departed the main discussions into two parts: one is about silicon-germanium hetero-junction

bipolar transistors, and the other one is the MOS transistors.

As discussed above, reliability stressing and burn-in of bipolar transistors historically proceeds along two different paths: reverse emitter-base stress, which is used to inject hot carriers (electrons or holes) into the E-B spacer oxide, thereby introducing generation/recombination (G/R) center traps, which lead to excess non-ideal base current and hence current gain degradation. The other one is forward-current density, which is as well as EB stressing, also results in current gain degradation under a high voltage or a high current stressing. Recently, due to the popularly used for SiGe HBTs in RF power amplifiers, the biasing condition which is simultaneously applying under a high  $V_{CB}$  voltage and a high collector current density is a new challenge to active devices. A new reliability damage mechanism which was termed as mixed-mode degradation was reported in SiGe HBTs. It results from the simultaneous application of high  $J_C$  and high  $V_{CB}$  and gets the hot carrier damage. In this thesis, we also discussed and analyzed this practical reliability mechanism in SiGe HBTs, especially for its RF power applications.

Typical stressing like under the E-B reverse biasing results in some traps near the E-B spacer oxide and interface states in EB junctions. Those effects result in a non-ideal G/R base leakage current thus decrease the output current gain. Since the hot carrier damage affects the base current but remains the collector current unaffected of SiGe HBTs, we discussed the different currents (constant  $I_C$  and constant  $I_B$ ) driving before and after stressing. In addition, by using a small-signal model, we extracted and compared the parameters before and after E-B reverse stressing. Then, we tried to find the co-relation and interaction between the DC parameter

degradations and the degradations of RF figures-of-merit. As to the mixed-mode stressing, a commercial large-signal (VBIC) model is used to examine the hot carrier damage on the high frequency characteristics of SiGe HBTs. We finally found that the device of SiGe HBT is more robust to hot carrier damage on high frequency and RF power performance when it is under the driving of a constant collector current.

In another part of this thesis, we discussed and analyzed the reliability issues on the high frequency characteristics of MOS transistors. The discussion and analysis of RF reliabilities in this thesis included the hot-carrier damage and the critical gate oxide breakdown of MOS transistors. In addition, the discussion covered the main specifications of high frequency applications of MOS transistors like the cutoff frequency, maximum oscillation frequency, noise figure, linearity, and RF power performance. In this experiment, we finally found that the DC reliability parameters are lack and can not fit and present the RF reliability degradations. So, a RF reliability model is urgent and suggested to be constructed, especially for the future application of RF circuits.



## 誌 謝

在完成論文的同時，回想起這些年來的求學階段，酸甜苦澀一點一滴彷彿時光倒流地浮現在我腦裡。我很慶幸，也很幸運的是每個階段帶給我的歡樂和成長總是大過於苦澀。在追求個人的目標當中，一路伴隨著我的除了我的親人，更要感謝的是那一群貴人和好朋友。首先要感謝的是我們最敬愛的老師，張俊彥院士；老師對台灣教育界和科技界的貢獻讓個人非常佩服和景仰，也將是學生這一生奮鬥的目標。學生能有幸畢業於老師門下，此時此刻是我這一生中最大的榮耀。我也非常感謝 NDL 的研究員，陳坤明博士、黃國威博士和簡昭欣博士，在你們的帶領之下，我們的情誼亦師亦友，除了課業方面之外，也讓我學到了許多待人處世的道理。尤其特別感謝陳坤明博士以及黃國威博士，無論在怎樣的情況下都是給予我最大的鼓勵和支持。當然也要謝謝 NDL 的工程師們在量測技術上給予的幫助。再來要感謝聯華電子的梁其翔副處長、曾誌裕經理、洪建州經理、林俊儀經理以及范政文經理，因為有你們的提攜和照顧讓我在生活上無匱乏。CYC 實驗室的陳經緯博士、吳師道博士、李宗霖博士、楊宗熺博士、吳永俊博士，彭辭修博士、陳漢譽博士以及羅文正學長，還有我的同學涂俊豪，芯卉學妹、怡誠學弟、兆欽學弟、伊喬助理以及所有 CYC 的成員，謝謝你們這些年來的相伴！最後

要感謝的是我的家人，爸爸、媽媽、岳父岳母謝謝你們的支持和鼓勵，  
當然還有最辛苦的老婆依齡，謝謝你生活上的照顧，讓我能專心地完成  
這個學業。 謝謝各位，祝福你們~

小懿

2007 六月于風城交大





# Contents

<i>Chinese Abstract</i>	<i>I</i>
<i>English Abstract</i>	<i>IV</i>
<i>Acknowledgement</i>	<i>VII</i>
<i>Contents</i>	<i>IX</i>
<i>Table Captions</i>	<i>XIII</i>
<i>Figure Captions</i>	<i>XIV</i>

## *Chapter 1 Introduction*

1.1 Overview of Transistors for RF Technologies	1
1.2 Issues on SiGe Hetero-junction Bipolar Transistors	1
1.2.1 Basic Concept of Hetero-junction Bipolar Transistor	2
1.2.2 Physical Improvements of HBTs	3
1.3 Introduction to RF CMOS Performance	5
1.4 Motivation	6
1.5 Thesis Organization	8

## *Chapter 2 Reliability Degradation Mechanisms in Si-Based Transistors*

2.1 Introduction to topic	13
---------------------------	----

2.2	Reliability issues on Si/SiGe Bipolar Transistors	13
2.2.1	Reverse Emitter-Base Junction Stressing (OC Stress)	14
2.2.2	Forward Collector-Base Junction Stressing (FC Stress)	15
2.2.3	Mixed-Mode Stressing (MM Stress)	16
2.3	Reliability issues on MOS Transistors	17
2.3.1	Hot Carrier Mechanism	17
2.3.2	Critical Gate-Oxide Breakdown Mechanism	19
2.4	Summary	20

***Chapter 3 Electrical Stress Effects on SiGe HBTs for High-Frequency Applications***

3.1	Introduction	26
3.2	Hot-Carrier Effects on High-Frequency Performance	27
3.3	Hot-Carrier Effects on RF Power Behavior	31
3.3.1.	RF Power Characteristics	32
3.3.2.	RF Linearity	33
3.4	Summary	35

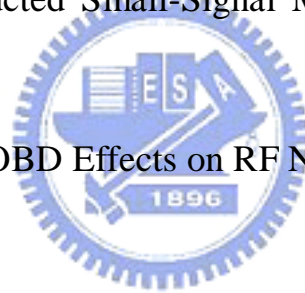
***Chapter 4 “Mixed-mode” Stress Effects on SiGe HBTs for High-Frequency and RF Power Applications***

4.1	Introduction	55
4.2	Mixed-mode Stress Effects on High-Frequency Performance	56
4.3	Mixed-mode Stress Effects on Power Performance	58
4.4	Device Modeling after Mixed-mode Stress	61

4.5	Summary	63
-----	---------	----

***Chapter 5 Characterization and Modeling of RF MOSFETs  
under Hot Carrier Stress and Oxide Breakdown***

5.1	Introduction of HCS and OBD on RF MOSFETs	79
5.2	HCS and OBD Experiments	80
5.3	Results and Discussion	80
5.3-1.	HCS Effects on the High-Frequency Performance of RF MOSFETs	81
5.3-2.	A Constructed Small-Signal Model of RF MOS transistors under OBD	83
5.3-3.	HCS and OBD Effects on RF Noise Figure	85
5.4	Summary	88



***Chapter 6 Impact of Reliability issues on Power Characteristics  
of RF MOS transistors***

6.1	Introduction	105
6.2	Experiments of HCS and OBD	105
6.3	Results and Discussion	106
6.3.1	<i>Hot Carrier Effects on Power Performance</i>	106
6.3.2	<i>Hot Carrier Effects on Linearity</i>	108
6.3.3	<i>Effects of oxide breakdown on RF Power Performance</i>	110
6.4	Summary	112

## ***Chapter 7 Conclusions and Suggestion for Future Work***

7.1 Conclusion	125
7.2 Suggestion for Future Work	127

<b><i>REFERENCES</i></b>	130
--------------------------	-----



# Table Captions

## Chapter 3

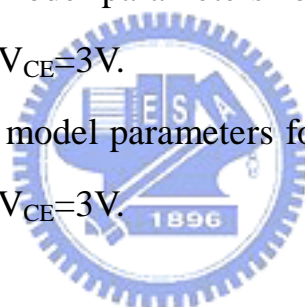
Table 3-I Equivalent hybrid- $\pi$  model elements for a typical SiGe transistor before and after stress.  $V_{CE} = 3V$ .

Table 3-II Summary of changes for the ideality factors, transconductance and RF linearity ( $IIP3$ ) for the base-current and collector-current before and after stress.

## Chapter 4

Table 4-I. Some VBIC model parameters for a SiGe transistor before and after stress.  $V_{CE}=3V$ .

Table 4-II. Some VBIC model parameters for a SiGe transistor before and after stress.  $V_{CE}=3V$ .



## Chapter 5

Table 5-1 Small-signal model parameters before and after HCS and OBD.

# Figure Captions

## Chapter 1

Fig. 1.1 Cross-section of a typical Si/SiGe HBT.

Fig. 1.2 The bandgap diagram of emitter and base junction in SiGe HBTs

Fig. 1.3 The bandgap in the base decreases toward the collector junction and a built-in field exists.

## Chapter 2

Fig. 2.1. The band diagram of an npn-Si/SiGe HBT under OC stress

Fig. 2.2. The band diagram of an npn-Si/SiGe HBT under FC stress

Fig. 2.3. The band diagram of an npn-Si/SiGe HBT under MM stress

Fig. 2.4: (a) Channel hot electrons (b) Drain avalanche hot carriers (c) Substrate hot electrons

Fig. 2.5: (a) Schematic illustrating the trapping of tunneling electrons. (b) Schematic illustrating the generation of an electron-hole pair in the anode by a tunneling electron. (c) Schematic illustrating the trapping of holes in the oxide layer.

## Chapter 3

Fig. 3.1. The band diagram of an npn-Si/SiGe HBT under OC stress.

Fig. 3.2 (a). Gummel plot of a typical SiGe transistor before and after stress. For power characterization, the collector current  $I_C$  and base current  $I_B$  are 52 mA and 0.34 mA, respectively, before stress. After stress,  $I_B$  changes to 0.7 mA under constant collector current measurement, while  $I_C$  changes to 24 mA for constant

base current measurement.

Fig. 3.2 (b) DC current gain ( $\beta$ ) measured before and after stress.

Fig. 3.3 (a) The measured S11 before and after stress at constant base-current and constant collector-current measurements.

Fig. 3.3 (b) The measured S22 before and after stress at constant base-current and constant collector-current measurements.

Fig. 3.3 (c) The measured S21 before and after stress at constant base-current and constant collector-current measurements.

Fig. 3.4 A simple equivalent hybrid- $\pi$  model of Si/SiGe HBT.

Fig. 3.5 (a) The  $|h_{21}|$  versus frequency before and after stress measured at a fixed collector current of 52mA.

Fig. 3.5 (b) The  $|h_{21}|$  versus frequency before and after stress measured at a fixed base current of 0.34mA.

Fig. 3.6 (a) Cutoff-frequency versus collector current measured before and after HC stress.

Fig. 3.6 (b) Cutoff-frequency versus base current measured before and after HC stress.

Fig. 3.7 (a) Linear power gain versus collector current before and after stress measured with  $P_{in} = -30\text{dBm}$ .

Fig. 3.7 (b) Linear power gain versus base current before and after stress measured with  $P_{in} = -30\text{dBm}$ .

Fig. 3.8 (a) Output power, power gain and PAE versus input power before and after stress measured at a fixed collector current.

Fig. 3.8 (b) Output power, power gain and PAE versus input power before and after stress measured at a fixed base current.

Fig. 3.9 Output power and third-order intermodulation power versus input power for a SiGe HBT before and after stress.



## Chapter 4

Fig. 4.1 Typical Gummel plot of a SiGe transistor under mixed-mode stress with different stressing times.

Fig. 4.2 An excess  $I_B$  leakage current component in reverse Gummel plot after mixed-mode stress.

Fig. 4.3 Cutoff-frequency versus collector current before and after stress.

Fig. 4.4 Maximum oscillation frequency versus collector current before and after stress.

Fig. 4.5 (a) Output power, power gain, and PAE versus input power before and after stress measured at fixed collector current (34mA).

Fig. 4.5 (b) Output power, power gain, and PAE versus input power before and after stress measured at fixed base current (40 $\mu$ A).

Fig. 4.6 (a) Output power and third-order intermodulation power versus input power for a SiGe HBT before and after stress under constant base-current measurement.

Fig. 4.6 (b) Output power and third-order intermodulation power versus input power for a SiGe HBT before and after stress under constant collector-current measurement.

Fig. 4.7 Measured and simulated forward Gummel plot of a SiGe HBT (a) before and (b) after stress.

Fig. 4.8 The current gain before and after stress.

Fig. 4.9 (a) A topology of Class-A power amplifier. (b) Measured and simulated output power, power gain, and PAE before stress with a collector current kept to a constant.

Fig. 4.10 Measured and simulated output power, power gain, PAE and IM3 after stress. The base current was kept to a constant.

Fig.4.11 Cross-section of SiGe HBT in this work.

## Chapter 5

Fig. 5.1 (a) DC characteristics of a MOSFET before and after hot carrier stress and oxide breakdown. (b) The threshold voltage measured with the HC stressing time.

Fig. 5.2 Output I-V characteristics of MOS transistor (a) after hot-carrier stress, (b) after oxide breakdown.

Fig. 3 Variations of the extracted transconductance and output conductance with increasing HC stressing time.

Fig. 5.4 S-parameters measured with the HC stressing time.

Fig. 5.5 Output impedance versus stress time at different bias condition.

Fig. 5.6 A constructed small-signal model for MOS transistor.

Fig. 5.7 Capacitance degradation with increasing HC stressing time.

Fig. 5.8 Relation between  $f_T$  and  $f_{max}$  degradations and  $g_m$  degradation.

Fig. 5.9 A re-constructed small-signal model for MOS transistor with the leakage current paths of  $R_{gs}$  and  $R_{gd}$ .

Fig. 5.10 (a) Cutoff frequency and (b) maximum oscillation frequency measured with the gate voltage before and after oxide breakdown.

Fig. 5.11 Relation between  $f_T$  and  $f_{max}$  degradations and  $g_m$  degradation after hot carrier stress and oxide breakdown.

Fig. 5.12 Minimum Noise Figure degradations before and after hot carrier stress and oxide breakdown with increasing (a) frequencies, (b)  $I_{DS}$ .

Fig. 5.13 (a) Equivalent linear lumped-element circuit for MOS transistor including noise sources. (b) Equivalent noiseless network with input referred voltage and current generators.

Fig. 5.14 (a) Equivalent noise resistance and (b) Optimized input reflection coefficient before and after HCS and OBD.

## Chapter 6

Fig. 6.1. Output characteristics of a MOSFET before and after HC stress. Output conductance ( $g_{ds}$ ) is determined from the slope of  $I_{DS}$ - $V_{DS}$  characteristics.

Fig. 6.2. Transconductance ( $g_m$ ) versus gate biases for a MOSFET before and after HC stress.

Fig. 6.3. Output power and third-order intermodulation power versus input power for a MOSFET before and after stress measured at a fixed  $V_{GS} = 0.8$  V.

Fig. 6.4. Power gain versus gate bias voltage for a MOSFET before and after stress measured at a fixed  $V_{DS} = 1.2$  V.

Fig. 6.5.  $VIP3$  versus  $V_{GS} - V_{TH}$  for a MOSFET before and after stress. Inset is the effective channel mobility before and after stress.

Fig. 6.6. Measured  $OIP3$  and  $IIP3$  versus drain current for a MOSFET before and after HC stress.

Fig. 6.7. Simulation results of  $VIP3$  with different subthreshold swings and mobility degradation coefficients.

Fig. 6.8 Power gain versus gate bias voltages for a MOSFET before and after oxide breakdown at a fixed  $V_{DS} = 1.2$  V.

Fig. 6.9 Output power, power gain and PAE versus input power before and after oxide

breakdown and HC stress.

Fig. 6.10 Measured  $OIP3$  and  $IIP3$  versus drain current for a MOSFET before and after oxide breakdown

Fig. 6.11 Measured  $g_{m3}$  versus gate-biases for a MOSFET before and after oxide breakdown

Fig. 6.12 Measured  $VIP3$  versus  $(V_{GS}-V_{TH})$  for a MOSFET before and after oxide breakdown

## Chapter 7

Fig. 7.1. Cross-section and layout design of one finger cell of “series-parallel” RF power MOS structure.

